Numerical Investigation of Fracture Channel Waves

Weidong Yi [1], Seiji Nakagawa [1], Kurt T. Nihei [2], James W. Rector [1], Larry R. Myer [2], & Neville G. W. Cook [1]

[1] *Materials Science & Mineral Engineering Department, 579 Evans Hall, University of California, Berkeley, CA 94720, USA*

[2] *Earth Sciences Division, E. O. Lawrence Berkeley National Laboratory, 1 Cyclotron Road, MS 90-1116, Berkeley, CA 94720, USA*

SUMMARY

This paper examines the characteristics of channel wave propagation in a waveguide formed by two parallel fractures using two-dimensional elastic finite difference simulation and mode analysis. Velocity dispersion of the fracture channel waves computed from f-k analysis of the synthetic waveforms shows good agreement with the mode solution. The dispersion characteristics of the fracture channel waves are compared to those for classic Rayleigh channel waves in a low velocity layer with properties selected so that the S-wave acoustic impedance of the layer matches that of the fracture waveguide at the central frequency of the source. Significantly different velocity-frequency behavior for the various modes was observed for the two types of waveguides. In addition, the fracture waveguide shows high-frequency thickness resonances in the vicinity of the source.

INTRODUCTION

In recent years, fractures in tight reservoir rocks have been recognized as major conduits for oil and gas production. Optimal well placement and production require a knowledge of characteristics such as fracture dimensions, aperture, and compliance. A basic challenge is to determine these geometrical and physical properties from seismic measurements.

Schoenberg (1980) and Pyrak-Nolte et al. (1987, 1990) have demonstrated that thin, compliant features such as fractures possess an acoustic impedance, $I_{frac} = \kappa/\omega$, which is different from the host rock, $I_{host} = \rho c$, where k is the fracture stiffness [stress/length], w is the angular frequency of the wave, and ρ and c are the density and velocity of the host rock. The impedance contrast between the fracture and host rock determines the seismic visibility of the fracture: $I_{host}/I_{frac} = (\rho c \omega)/\kappa$. This relation shows that the seismic visibility of the fracture is dependent on both its stiffness and the frequency of the wave, the effect being largest when the fracture stiffness is low compared to the product of the acoustic impedance of the host rock times the frequency of the wave.

Because fractures possess a frequency-dependent acoustic impedance, a variety of interesting elastic wave phenomena have been demonstrated to exist for wave propagation across and along single fractures. These effects include frequency-dependent transmission and reflection, including wave conversions, and dispersive fracture interface wave propagation. Since fractures typically appear as sets of nearly parallel planar features, it is of importance to determine the seismic response of waves traveling between fractures. The objective of this paper is to demonstrate that parallel fractures form an elastic waveguide that supports a family of channel waves which can be viewed as generalized Rayleigh-Lamb plate waves for the case when the plate is sandwiched between two halfspaces through normal and tangential springs. in addition, several interesting properties of fracture channel waves which differ from conventional Rayleigh channel waves supported by a low velocity layer are shown for the first two lowest order symmetric modes.

ELASTIC FINITE DIFFERENCE CODE FOR FRACTURED ROCK

Numerical simulations of elastic wave propagation in a medium with two parallel fractures were performed using a two-dimensional, elastic, staggered grid finite difference code (Virieux, 1986) code which uses fourth-order differencing in space, and second-order differencing in time (Levander, 1988). Fractures can be integrated into the finite difference code either as cells with anisotropic properties chosen to exactly replicate the normal and tangential fracture stiffnesses or by explicitly applying the displacement-discontinuity boundary conditions across neighboring grid cells (Coates and Schoenberg, 1995). For fractures that are aligned with the finite difference grid, the latter approach is the simplest and is the approach used in this paper.

For a planar fracture located in the *x-y* plane, the displacement-discontinuity boundary conditions for a fracture are (Schoenberg, 1980; Pyrak-Nolte et al., 1990):

$$u_x^+ - u_x^- = \frac{\tau_{zx}}{\kappa_{zx}}, \qquad u_z^+ - u_z^- = \frac{\tau_{zz}}{\kappa_{zz}} \qquad (1)$$

$$\tau_{zz}^+ = \tau_{zz}^-, \qquad \tau_{zx}^+ = \tau_{zx}^- \qquad (2)$$

where u is the particle displacement, τ is the stress, and κ is the fracture stiffness in units of [Pa/m], and the superscripts + and - refer to opposite sides of the fracture. The displacement-discontinuity boundary conditions are a generalized boundary condition in the sense that they degenerate to the boundary condition for a welded interface as $\kappa \to \infty$ and for a free-surface as $\kappa \to 0$. Laboratory ultrasonic measurements of wave transmission across a single fracture (Pyrak-Nolte et al., 1990; Hsu and Schoenberg, 1988) and fracture interface wave propagation along a single fracture (Pyrak-Nolte et al., 1992; Roy and Pyrak-Nolte, 1995) have demonstrated that this model provides a good description of the dynamic behavior of a fracture.

NUMERICAL SIMULATIONS

Numerical Model

The geometry of the models used for numerical simulations are (a) for a fracture waveguide; two parallel fractures with identical stiffness embedded in a homogeneous background medium and spacing between fractures is 2λ (P-wave wavelength λ) and (b) for a velocity-contrast waveguide with layer thickness and P- and S-wave transmission coefficients identical to case (a). For both waveguides, a single explosion source with a central frequency of 374Hz was located at the center of the layers. The velocity of the source was provided by the first derivative of a Gaussian function. Absorbing boundary conditions were applied along all four boundaries of the computational domain.

For the fracture waveguide, fractures were modeled by internal boundaries with displacement-discontinuity boundary conditions. Normal and tangential stiffnesses of the fractures were assumed to be identical ($\kappa_{zx} = \kappa_{zz}$). Two different stiffnesses were used for simulations, one yielding a normal incident P-wave transmission coefficient (at 374 Hz) equal to 0.6 ($\kappa_{zx} = \kappa_{zz} = 7.8 \times 10^9$ Pa/m) and the other a transmission coefficient equal to 0.9 ($\kappa_{zx} = \kappa_{zz} = 2.2 \times 10^{10}$ Pa/m). Spacing between the fractures was set to twice the P-wave wavelength at 374 Hz. The density of the host medium was 2000 kg/m^3; P- and S-wave velocities were 3740 m/sec and 2496 m/sec, respectively.

Numerical simulations were also conducted for a low velocity layer bounded by upper and lower half-spaces with identical material properties. Both the layer thickness and properties were chosen identical to those of the fracture waveguide. For the halfspaces, the material density was fixed and the P- and S-wave velocities increased to give the same normal incidence transmission coefficients used in the fracture waveguide simulations.

Snapshots

Snapshots taken at t=62 msec for the P-wave transmission coefficient of 0.6 case for both types of waveguides are shown in Figure 1. It can be seen that the velocity-contrast waveguide traps the wave energy more efficiently than the fracture waveguide. For the fracture waveguide, the wavefront outside the layer propagates slightly slower than inside the layer due to the frequency-dependent time delay the wave experiences as it crosses the fracture.

The wavefield around the fracture waveguide is also characterized by strong head waves. The head waves are generated as a result of interaction between the propagating P-wave wavefront inside and outside the waveguide and fractures. For the velocity-contrast waveguide, no significant head waves were generated.

Snapshots for the vertical component of the waves (Fig. 1b) show strong high-frequency reverberation near the source in the fracture waveguide. This is due to the reflection of high-frequency waves by the fracture. The velocity-contrast waveguide, on the other hand, does not show such reverberations.

Dispersion Analysis

For both the fracture and velocity-contrast waveguide, a channel wave in the waveguide consists of multiple modes with different velocities. Therefore, by examining the dispersion relations in a measured seismogram, the modal structure of the wave can be determined.

For this purpose, an array of receivers were located along the center of the waveguides 12 wavelengths from the source. By applying f-k (frequency-wavenumber) analysis to the seismograms measured at different horizontal offsets, the velocity dispersion of the wave can be computed. The synthetic seismograms and corresponding f-k plots for both waveguides are shown in Figure 2 and Figure 3 for the 0.6 transmission coefficient case. In the f-k plots, the slope of each curve represents the velocity dispersion behavior of the various channel wave modes. The modal structure of wave for the fracture waveguide can be seen clearly. However, for the velocity-contrast waveguide, individual modes cannot be clearly distinguished. It is also noticed that the fracture channel waves high frequencies than the velocity contrast waveguide.

The phase velocities for the lowest-order symmetric mode are shown in Figure 4, also shown are the analytic predictions obtained from mode analysis (Nihei et al., 1998). Good agreement between the numerical and mode analysis results demonstrates the accuracy of the numerical code. Mode analysis of the fractured waveguide shows the fracture channel waves to be generalized Rayleigh-Lamb plate waves. This simulation confirms that such waves can be generated by a simple point explosion source, as should be expected.

To examine the characteristics of the wavefield of the fracture waveguide near the source, the receiver array was moved to four wavelengths from the source. f-k analysis of the wavefield reveals the existence of leaky modes that result from multiply reflected waves (Fig. 5). The phase velocities of these leaky modes can be seen to be extensions of the true normal modes above the shear wave velocity. Because of the finite offset between source and receiver, it is not possible to see the continuation of these waves to near vertical incidence, as present in the snapshot in Figure 1. The complexity of the wavefield near the source in the fracture waveguide results from the frequency-dependent reflectivity of multiple parallel fractures.

CONCLUSIONS

This numerical investigation demonstrates that the velocity dispersion of the fracture channel waves computed from f-k analysis of the synthetic waveforms is in good agreement with the mode solution. The fracture channel waves are shown to be generalized Rayleigh-Lamb plate modes that propagate as normal modes below the shear wave velocity and as leaky modes above the shear wave velocity.

The dispersion characteristics of the fracture channel waves are compared to those for classic Rayleigh channel waves in a low velocity layer with properties selected such that the S-wave acoustic impedance of the layer match that of the fracture waveguide at the central frequency of the source. Significantly different velocity-frequency behavior for the various modes was observed for the two types of waveguides; in addition, the fracture waveguide shows high-frequency thickness resonances near the source. These differences can be attributed to the frequency-dependent acoustic impedance of the fractures.

REFERENCES

Levander, A. R. (1988). Fourth-order finite-difference P-SV seismograms, Geophysics, 53, 1425-1436.

Nihei, K.T., W. Yi, L.R. Myer, and N.G.W. Cook (1998). Fracture channel waves, J. Geophys. Res. (submitted).

Hsu, C. J. an d Schoenberg M. (1993). Elastic waves threough a simulated fractured medium, Geophysics, 58:7, 964-977

Pyrak-Nolte, L. J. (1988) Seismic visibility of fractures, Ph.D. Dissertation, Dept. of Mater. Sci. and Miner. Eng. Univ. of Calif., Berkeley

Pyrak-Nolte, L. J., L. R. Myer, and N. G. W. Cook. (1990). Transmission of seismic waves across single natural fractures, J. Geophys. Res., 95:B6, 8617-8638.

Pyrak-Nolte, L. J., J. Xu, and G. M. Haley. (1992). Elastic interface waves propagating in a fracture, Phys. Rev. Lett., 68, 3650-3653.

Roy, S. and L. J. Pyrak-Nolte. (1995). Interface waves propagating along tensile fractures in dolomite, Geophys. Res. Lett., 22:20, 2773-2776.

Schoenberg, M. (1980). Elastic wave behavior across linear slip interfaces, J. Acoust. Soc. Am., 68:5, 1516-1521.

Virieux, J. (1986). P-SV wave propagation in heterogeneous media: Velocity-stress finite-difference method, Geophysics, 51:4, 889-901.
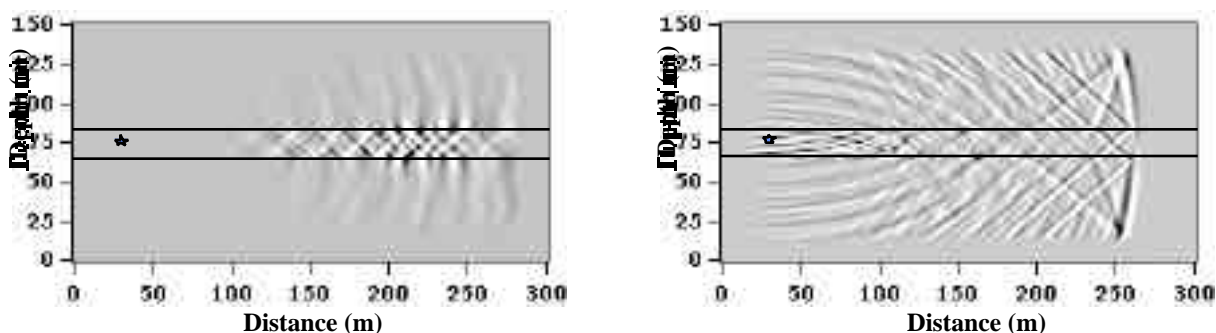
Figure 1 Examples of snapshots taken at t=62msec for waves propagating in (left) velocity-contrast and (right) fracture waveguides. P-wave transmission coefficient of the boundaries between waveguides and the surrounding medium is T=0.6. Location of the explosion source is indicated by a star.
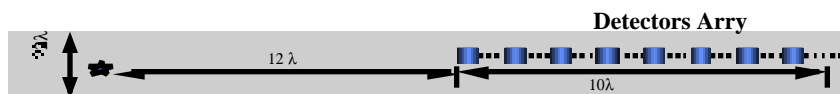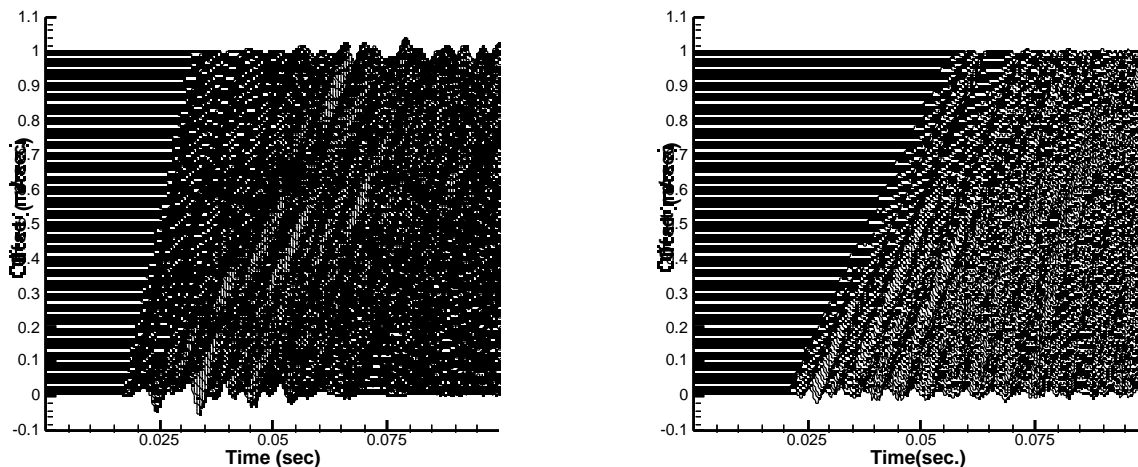

Figure 2 Examples for vertical components of velocities measured at far field (receivers farther than 12 wavelengths from the source) for (left) the velocity-contrast and (right) fracture waveguides with transmission coefficient of 0.6.
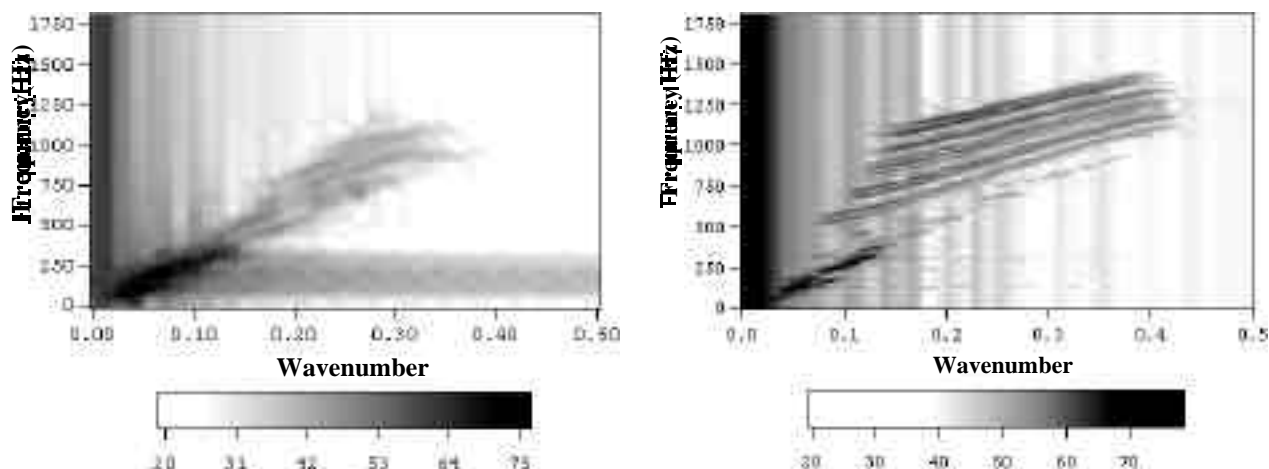
Figure 3 Examples for f-k diagram at far-field for (left) velocity contrast waveguide and (right) fracture waveguide with P-wave transmission coefficient of T=0.6. The spectra were computed from the seismogram measured at far-field shown in Figure 2.
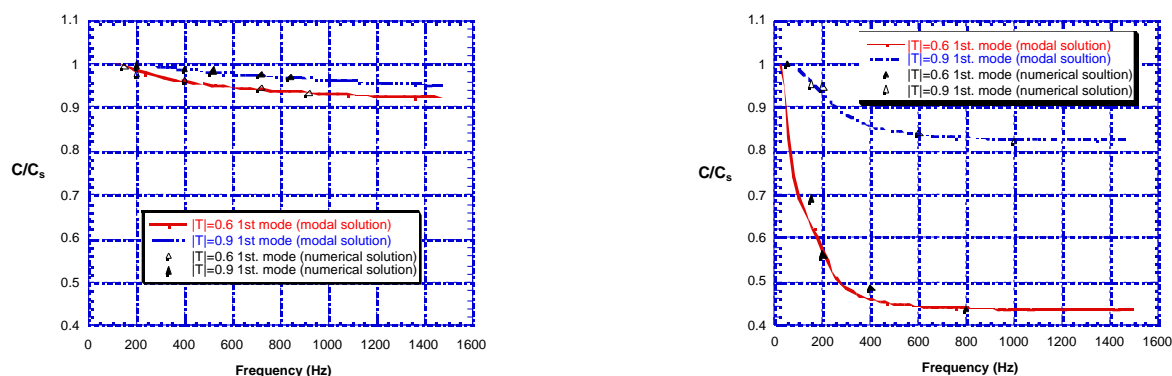
Figure 4 Phase velocity dispersion at far-field for fracture waveguide obtained by f-k analysis. Dispersion relation from the numerical simulations are shown by solid (transmission coefficient T=0.9) and open (T=0.6) triangles. Analytic modal solutions from a plane wave analysis are also shown in solid line (T=0.6) and broken line (T=0.9).
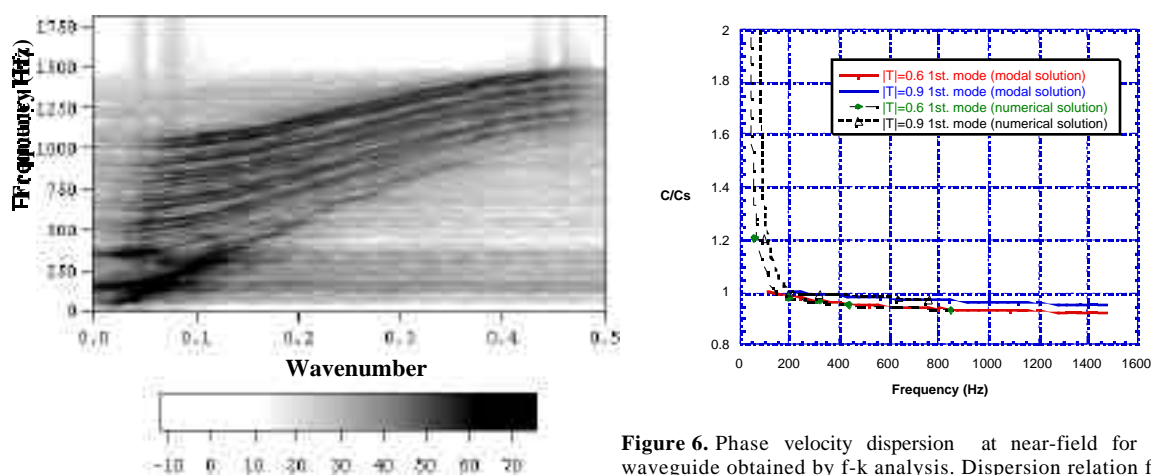
Figure 5 f-k analysis for the fracture waveguide with a transmission coefficient of 0.6 an array of receivers located along the center of the waveguides for four wavelengths from the source

Figure 6. Phase velocity dispersion at near-field for fracture waveguide obtained by f-k analysis. Dispersion relation from the numerical simulations are shown by solid (transmission coefficient T=0.6) and open (T=0.9) triangles with dash line. Analytic modal solutions from a plane wave analysis are also shown in solid line (T=0.6 and 0.9).